Jiang et al. *Zool. Res.* 2024, 45(2): 367−380
https://doi.org/10.24272/j.issn.2095-8137.2023.371

ZR | Zoological Research

Article Open Access

Potential therapeutic role of spermine via Rac1 in osteoporosis: Insights from zebrafish and mice

Rui-Xue Jiang[1,2,#], Nan Hu[2,3,#], Yu-Wei Deng[1,2], Long-Wei Hu[2,4], Hao Gu[1,2], Nan Luo[2,5], Jin Wen[1,2,*], Xin-Quan Jiang[1,2,*]

[1] *Department of Prosthodontics*, *Shanghai Ninth People's Hospital*, *Shanghai Jiao Tong University School of Medicine*, *Shanghai* 200011, *China*

[2] *College of Stomatology*, *Shanghai Jiao Tong University*; *National Center for Stomatology*; *National Clinical Research Center for Oral Diseases*; *Shanghai Key Laboratory of Stomatology*; *Shanghai Research Institute of Stomatology*; *Shanghai Engineering Research Center of Advanced Dental Technology and Materials*, *Shanghai* 200125, *China*

[3] *Department of Endodontics*, *Shanghai Ninth People's Hospital*, *Shanghai Jiao Tong University School of Medicine*, *Shanghai Jiao Tong University*, *Shanghai* 200011, *China*

[4] *Department of Oral and Maxillofacial-Head and Neck Oncology*, *Shanghai Ninth People's Hospital*, *School of Medicine*, *Shanghai Jiao Tong University*, *Shanghai* 200011, *China*

[5] *Department of Preventive Dentistry*, *Shanghai Ninth People's Hospital*, *Shanghai Jiao Tong University School of Medicine*, *Shanghai Jiao Tong University*, *Shanghai* 200011, *China*

ABSTRACT

Osteoporosis (OP) is a prevalent metabolic bone disease. While drug therapy is essential to prevent bone loss in osteoporotic patients, current treatments are limited by side effects and high costs, necessitating the development of more effective and safer targeted therapies. Utilizing a zebrafish (*Danio rerio*) larval model of osteoporosis, we explored the influence of the metabolite spermine on bone homeostasis. Results showed that spermine exhibited dual activity in osteoporotic zebrafish larvae by increasing bone formation and decreasing bone resorption. Spermine not only demonstrated excellent biosafety but also mitigated prednisolone-induced embryonic neurotoxicity and cardiotoxicity. Notably, spermine showcased protective attributes in the nervous systems of both zebrafish embryos and larvae. At the molecular level, Rac1 was identified as playing a pivotal role in mediating the anti-osteoporotic effects of spermine, with P53 potentially acting downstream of Rac1. These findings were confirmed using mouse (*Mus musculus*) models, in which spermine not only ameliorated osteoporosis but also promoted bone formation and mineralization under healthy conditions, suggesting strong potential as a bone-strengthening agent. This study underscores the beneficial role of spermine in osteoporotic bone homeostasis and skeletal system development, highlighting pivotal molecular mediators. Given their efficacy and safety, human endogenous metabolites like spermine are promising candidates for new anti-osteoporotic drug development and daily bone-fortifying agents.

Keywords: Osteoporosis; Spermine; Rac1; Zebrafish; Mice

INTRODUCTION

Osteoporosis (OP) is a prevalent metabolic bone disorder characterized by reduced bone mass and deterioration of bone tissue microstructure (Gopinath, 2023), leading to chronic pain, deformity, and restricted activity. With an increasing aging population globally, OP has become a significant public health issue, placing immense pressure on healthcare systems (Abtahi et al., 2018; Kemmak et al., 2020). Although drug therapy is critical for mitigating bone loss and preventing fragility fractures in OP patients, existing treatments are limited. Bisphosphonates (BPs), primary anti-bone resorptive agents, have proven effective in various studies (Black et al., 1996; Yamasaki, 2023), but their prolonged use can cause serious complications, such as medication-related osteonecrosis of the jaw (MRONJ) (Kim et al., 2021; Wat, 2016). While bone formation drugs like teriparatide offer potential benefits (Yuan et al., 2023), they

Received: 26 November 2023; Accepted: 15 January 2024; Online: 16 January 2024

Foundation items: This work was supported by the National Natural Science Foundation of China (81921002, 81900970, 82130027), Innovative Research Team of High-Level Local Universities in Shanghai (SHSMU-ZLCX20212400), and Young Physician Innovation Team Project (QC202003) of Ninth People's Hospital affiliated to Shanghai Jiao Tong University School of Medicine. Shanghai "Rising Stars of Medical Talent" Youth Development Program is also acknowledged

[#]Authors contributed equally to this work

*Corresponding authors, E-mail: xinquanjiang@aliyun.com; echomet@126.com

also exhibit limited clinical utility due to their complex delivery, prohibitive cost, and osteosarcoma risks (Kellier-Steele et al., 2022; Krege et al., 2022). These challenges highlight the urgent demand for novel anti-OP medications and further research efforts.

Endogenously produced metabolic molecules integral to human physiological processes have garnered attention as potential therapeutic agents (Das, 2021; Xiao et al., 2020). Spermine (SPM), an *in vivo* synthesized polyamine derived from putrescine and S-adenosyl-L-methionine, originates from intestinal microorganisms, endogenous cellular processes, and dietary sources (Sagar et al., 2021). SPM exhibits a broad spectrum of biological effects on cell proliferation (Xu et al., 2023), oxidative stress (Vrijsen et al., 2020), tumor growth (Li et al., 2023b), autophagy (Vrijsen et al., 2023), and inflammation (Cao et al., 2017; Jiang et al., 2021a). Notably, a decline in blood SPM levels has been observed in individuals aged between 60 and 80 years, whereas centenarians maintain higher levels (Pucciarelli et al., 2012). This molecule also exhibits potential in metabolic disease management, as demonstrated by the significant weight reduction observed in high-fat diet-induced obese mice following its supplementation (Sadasivan et al., 2014).

Preliminary research on the relationship between SPM and the skeletal system has found that warmer environments can lead to an increase in polyamine production by gut microbiota, thereby enhancing bone strength (Chevalier et al., 2020), with SPM also found to reduce cartilage and mineralized bone degradation in arthritic rats (Iezaki et al., 2012). In addition, mutations or deletions in the specific SPM synthase gene (*SMS*) have been reported to lead to skeletal dysplasia and OP, further highlighting the crucial role of SPM in bone homeostasis (Pegg, 2014). However, the definitive role of SPM in osteoporotic bone homeostasis and its underlying molecular mechanisms have not yet been fully revealed.

Zebrafish (*Danio rerio*) share more than 80% genetic similarity to humans (MacRae & Peterson, 2015) and are listed by the National Institutes of Health (NIH) as a leading vertebrate model, after humans and mice. Given their attributes, zebrafish have increasingly been employed for studying skeletal diseases and anti-OP drugs (Lin et al., 2022; Wang et al., 2018; Xie et al., 2023; Yin et al., 2019), optimizing screening efficiency and research costs.

In the current study, we explored the hypothesis that SPM positively regulates osteoporotic bone homeostasis. Using a zebrafish larval model of OP, we revealed a dual mechanism of SPM in alleviating OP through the promotion of bone formation and reduction of bone resorption. Furthermore, we identified the importance of the Rac1-P53 axis in mediating the anti-osteoporotic effects of SPM. This study assessed the potential of SPM as an innovative anti-OP agent, offering insights for its clinical development in targeted OP therapy.

MATERIALS AND METHODS

Zebrafish experiments

Adult wild-type (Tubingen line) and Tg (*ola.sp7:nlsGFP*) zebrafish were raised and maintained following standard protocols for embryo production (Guo et al., 2023; Huang et al., 2018). Fish were housed in a recirculating water system, with 15 zebrafish per tank, under a 14 h/10 h light/dark phase at a room temperature of 28.5°C. Zebrafish embryos and larvae were cultured in egg water containing sea salt and methylene blue (10 L ddH_2O+0.54 g sea salt+100 μL methylene blue). Female and male zebrafish were paired in a 1:1 or 2:1 ratio on the night before embryo collection. Spawning occurred the following day after 20 min of light exposure.

Larvae were used to establish an OP animal model. Two-day-old embryos (2 days post-fertilization (dpf)) were transferred into 6-well plates, with 30 larvae per well, for one day of adaptive culture. Based on previous studies and the developmental characteristics of zebrafish bones (Barrett et al., 2006; Dietrich et al., 2021; He et al., 2018; Jiang et al., 2021b), we used 25 μmol/L prednisolone (PN) (P829930, MACKLIN, China) from 3 to 7 dpf to induce OP. Dimethyl sulfoxide (DMSO) (D2650, Sigma-Aldrich, USA) was used as a control. The PN was dissolved with the appropriate amount of DMSO, and a high-concentration stock solution was prepared with egg water. Solutions were refreshed daily, and paramecia feedings began from 5 dpf. For testing the anti-OP effects of SPM, different concentrations (1 nmol/L, 10 nmol/L, 100 nmol/L) of SPM (S4624, Sigma-Aldrich, USA) and PN were added simultaneously, and larvae were harvested for examination on day 7. SPM was dissolved and diluted in egg water to the target concentrations. The Rac1 inhibitor 1A-116 (E2400, Selleck, USA) was prepared as a 10 μmol/L solution using egg water.

Rac1 knockdown was achieved using CRISPR interference (CRISPRi) technology. Rac1-single guide RNAs (sgRNAs) were first designed using the CCTop-CRISPR/Cas9 target online predictor tool (https://cctop.cos.uni-heidelberg.de/). Polymerase chain reaction (PCR) products were purified and used for *in vitro* sgRNA transcription. All operations were protected from RNase. Four *rac1*-sgRNAs (Supplementary Table S1) were combined with dCas9-EVE mRNA (final concentration of 200 ng/L) (YSY; China) and microinjected into embryos. The microinjection was completed within 30 min post-fertilization to ensure embryos were still at the single-cell stage. Administration of all agents in zebrafish larvae was performed on 3–7 dpf, with bone phenotypic and behavioral tests carried out on day 7.

Fresh zebrafish embryos (0 hours post-fertilization (hpf)) were used for the embryonic development experiments. PN and/or SPM were added based on group assignments, and solutions were renewed daily. Morphological observations were made every 12 h during the rapid development period (0–72 h), noting embryo mortality. The frequency of autonomic embryo movements was recorded under a stereomicroscope (DP74, OLYMPUS, Japan) at 24 hpf, and the heartbeat over 15 s at 48 hpf was also monitored to assess potential neurotoxicity and cardiotoxicity.

Alizarin red staining (ARS)

Zebrafish larvae (7 dpf) were fixed in 4% paraformaldehyde (PFA) for 2 h, rinsed in egg water, dehydrated in 50% ethanol, stained overnight in 0.5% Alizarin red staining solution, and bleached with a hydrogen peroxide/KOH solution. The larvae were then rinsed and stored in a glycerol/KOH solution at 4°C. Imaging was performed using a stereomicroscope (DP74, OLYMPUS, Japan), with quantitative analysis performed using ImageJ software.

Calcein staining

Adapting a method from an earlier study (Peng et al., 2022), zebrafish larvae at 7 dpf were stained with 0.2% calcein (C0875, Sigma-Aldrich, USA) and rinsed with egg water.

Imaging was performed using a fluorescence stereomicroscope (SMZ25, Nikon, Japan) and ImageJ was used for analysis.

_Sp7_ expression examination

Tg (*ola.sp7: nlsGFP*) transgenic zebrafish (Tg (sp7: EGFP)) were used to investigate the expression of *sp7*, an osteoblast-specific transcription factor essential for osteoblast proliferation, differentiation, and bone formation (Chen et al., 2019; Niu et al., 2017). Anesthetized 7 dpf larvae were imaged with a stereomicroscope (SMZ25, Nikon, Japan) and quantified using ImageJ.

RNA extraction, reverse transcription-quantitative real-time polymerase chain reaction (RT-qPCR)

Zebrafish embryos or larvae were homogenized in 1.5 mL microcentrifuge tubes containing 1 mL of TRIzol (T9424, Sigma-Aldrich, USA) using grinding rods. After 15 min of lysis, 200 μL of chloroform was added, followed by 10 min of incubation on the ice. Samples were centrifuged for 15 min at 12 000 r/min (radius of rotor=84 mm) and 4°C. The supernatant (500 μL) was then collected, combined with an equal volume of isopropanol, and centrifuged similarly. The resultant precipitates were sequentially washed with 75% ethanol and 99% ethanol. The purified RNA was resuspended in 20 μL of diethyl pyrocarbonate (DEPC) water. For RT-qPCR, the RNA was reverse transcribed using the Prime Script RT Master Kit (RR036A, TaKaRa, Japan). RT-qPCR was performed using the Roche LightCycler 480 system (v.1.5.1.74) with SYBR Green-based detection (1725270, Bio-Rad, USA), with β-actin used as an internal control. Primer sequences are provided in Supplementary Table S2.

Zebrafish histological sections preparation and staining

Zebrafish larvae (7 dpf) were fixed with 4% PFA overnight at 4°C. Subsequent steps involved gradient ethanol dehydration, dimethyl benzene clearance, and paraffin embedding. Sections (5-μm thick) were dried at 50°C for 30 min, then stained using a Hematoxylin-Eosin (H&E) Staining Kit (G1121; Solarbio, China) for tissue morphology and tartrate-resistant acid phosphatase (TRAP) staining (G1492, Solarbio, China) to measure osteoclast activity. Imaging was performed using a Zeiss Axio Scope A1 Microscope (ZEISS, German) with DP2-TWAIN software (v.3.0.0.6212).

RNA-sequencing (RNA-seq) and analysis

Zebrafish larvae (7 dpf) from the OP and OP+SPM groups were collected for RNA-seq. Total RNA was extracted following the manufacturer's instructions. RNA integrity was assessed by agarose gel electrophoresis (28S:18S≥1.5) and RNA purity was checked using a Nanodrop spectrophotometer (Nano–500, Allsheng, China) (OD260/280 ratio between 1.8–2.2) and quantified with Qubit (≥500 ng). The samples were sequenced using the Illumina NovaSeq 6000 platform (USA). Skewer software was used to trim splice sequences and low-quality fragments. According to the experimental design, differentially expressed genes (DEGs) between groups were identified with DESeq2 based on $|\log_2 FC| \geq 1$ and $P \leq 0.05$ criteria. Known gene expression was gauged using Fragments Per Kilobase of transcript per Million fragments mapped (FPKM). Gene Ontology (GO) and Kyoto Encyclopedia of Genes and Genomes (KEGG) enrichment analyses were performed for differential gene sets.

Ingenuity pathway analysis (IPA)

Differential gene datasets were analyzed using IPA software (Qiagen, China) to elucidate potential molecular networks, diseases, functions, and upstream regulators. A *P*-value threshold of <0.05 was set for all analyses.

Total protein extraction and western blotting

Zebrafish larvae (7 dpf) were twice washed with pre-chilled phosphate-buffered saline (PBS) before being lysed with radio immunoprecipitation assay (RIPA) lysis buffer (P0013B, Beyotime, China), supplemented with protease and phosphatase inhibitors and phenylmethylsulfonyl fluoride (PMSF). Samples were sonicated using an ultrasonic processor (VCX 130, SONICS, USA), incubated for 15 min on the ice, and centrifuged at 15 000 r/min (radius of rotor=84 mm) at 4°C for 20 min. The supernatants were transferred to new Eppendorf (EP) tubes and combined with lithium dodecyl sulfate (LDS) sample buffer (LT101S, Epizyme, China), followed by boiling at 100°C for 10 min. Western blotting was performed using standard protocols and signals were detected using the UVITEC Alliance system (v.16.0.3.0) and analyzed using ImageJ. Antibodies included: RAC1 rabbit polyclonal antibody (AF7854, Beyotime, China, 1:1 000), P53 mouse monoclonal antibody (2524T; Cell Signaling Technology; USA; 1:1 000), phospho-p53 (Ser15) antibody (9284T; Cell Signaling Technology; USA; 1:1 000), β-actin rabbit monoclonal antibody (8457T; Cell Signaling Technology; USA; 1:1 000), horseradish-peroxidase (HRP)-conjugated AffiniPure goat anti-rabbit IgG(H+L) (SA00001-2; Proteintech; China; 1:5 000), and HRP-conjugated AffiniPure goat anti-mouse IgG(H+L) (SA00001-1; Proteintech; China; 1:5 000).

Behavioral test

For the behavioral test, drug intervention began on day 3. Zebrafish larvae were continuously treated with 25 μmol/L PN or 25 μmol/L PN and 10 nmol/L SPM at 3–7 dpf. The solution was renewed daily, and paramecia feeding started at 5 dpf. Zebrafish larvae (7 dpf) were individually placed into 24-well plates containing 1 mL of egg water per well (Chen et al., 2022). After a 30 min accommodative period, larval swimming during light-to-dark transitions (three 5 min dark/light cycles) was monitored using the DanioVision™ system (Noldus, Netherlands). Heatmaps, trajectory plots, speed in different phases, average moving speed, total moving distance, distance from the center, and state of motion were calculated and analyzed.

Mouse experiment

Six-week-old male C57BL/6 mice (*Mus musculus*) were acclimated for one week before the study. Mice in the SPM group were gavaged daily with SPM (0.6 μmol/g/d) for three consecutive weeks, with the control group receiving saline (Con). At 10 weeks, bone mineral density (BMD) scans were conducted and analyzed (Lunar PIXImus II, GE, China).

Microcomputed tomography (micro-CT)

Femurs from mice in the Con and SPM groups were excised, fixed in 4% PFA for 24 h, and stored in 70% ethanol. Micro-CT scans were performed using the μCT 50 system (SCANCO Medical AG, Switzerland). Images were reconstructed to visualize three-dimensional structures. Analysis focused on the region below the growth plate.

H&E staining

Decalcified mouse femur samples underwent a similar processing and staining sequence as detailed for the zebrafish histological section preparation. Bone trabecular areas in the

region of interest (ROI) were analyzed using ImageJ.

Ethics statement

All experiments involving zebrafish and mice were approved by the Institutional Animal Care and Use Committee at the Ninth People's Hospital, School of Medicine, Shanghai Jiao Tong University (SH9H-2023-A843-1, SH9H-2019-A638-1).

Statistical analysis

Statistical analysis was conducted using GraphPad Prism v.9.0 software (San Diego, USA). All measurements are presented as mean±standard deviation (SD). Data distribution was confirmed using normality and lognormality tests. Appropriate statistical tests were applied based on data distribution, with $P<0.05$ considered significant.

RESULTS

SPM improves PN-induced OP in zebrafish larvae

To determine whether SPM can affect OP, we modeled OP in zebrafish larvae based on PN administration, as shown in Figure 1A. Alizarin red and calcein staining showed reduced notochord mineralization, while RT-qPCR analysis demonstrated altered osteoblast and osteoclast-related gene expression, suggesting successful establishment of the OP model (Figure 1B, C). Different concentrations of SPM (0, 1, 10, and 100 nmol/L) were used to intervene in the development of OP in the larvae (Figure 1D). Results showed that the addition of SPM significantly enhanced both the mineralized area and mean mineralized intensity, especially at 10 nmol/L (Figure 1E). The H&E staining results showed abnormal skeletal morphology in the OP group, characterized by spinal contracture and disturbed skeletal muscle cell arrangement. SPM ameliorated these skeletal abnormalities and partially restored skeletal muscle thickness (Supplementary Figure S1A). At the cellular level, SPM enhanced the expression of *sp7* in the maxillofacial bones of Tg (sp7: EGFP) zebrafish larvae under PN induction and up-regulated the expression of osteoblast-related markers (*runx2a*, *ocn*, *sp7*, *alpl*) (Figure 1F–H), demonstrating a positive role in promoting bone formation. Simultaneously, SPM also displayed an inhibitory effect on bone resorption, as evidenced by TRAP staining and analysis of osteoclast-related genes (*mmp9*, *acp5a*, *ctsk*, *mmp13a*, *rankl*) (Figure 1I–K). These observations suggest that SPM can improve PN-induced OP in zebrafish larvae by facilitating bone formation and suppressing bone absorption.

Rac1 and P53 may play a pivotal role in the anti-OP effects of SPM

After identifying its anti-OP effects, RNA-Seq was conducted to further explore the molecular mechanisms of SPM. Striking differences in gene expression were observed between the OP and OP+SPM groups based on principal coordinate analysis (PCA) and heatmap analysis (Figure 2A, B). Of the 320 DEGs identified ($\log_2|FC|\geq1$ and $P\leq0.05$ as inclusion criteria), 249 were co-expressed in both groups, 44 were unique to the OP group, and 27 were unique to the OP+SPM group (Figure 2C). From their expression trends, 117 DEGs were up-regulated and 203 DEGs were down-regulated after SPM intervention (Figure 2D). To verify the accuracy of RNA-Seq, we screened DEGs potentially related to skeletal system development and mineralization based on their absolute $\log_2$FoldChange value from highest to lowest. Quantitative measurements of representative genes were consistent with those from RNA-Seq, suggesting excellent accuracy (Figure 2E). The classical osteogenic-related Wnt signaling pathway was significantly up-regulated in KEGG enrichment analysis, ranking second. Correspondingly, the NF-kappa B signaling pathway, known to play an essential role in the differentiation and function of osteoclasts, was largely down-regulated after the addition of SPM, indicating a decrease in bone resorption activity. KEGG enrichment analysis also indicated that SPM activated the neuroactive ligand-receptor interaction signaling pathway, inducing some neuroprotective effects (Figure 2F).

IPA was next employed to further explore DEGs and master regulators identified through RNA-Seq (Figure 2G), highlighting Rac1 and TP53 (P53) as potential mediators of the therapeutic effects of SPM (Figure 2H). Rac1, a member of the small G protein family, and activation of the G protein-coupled receptor signaling pathway were also clarified based on GO enrichment analysis (Supplementary Figure S1B). Further examination of the relationship between Rac1 and P53 showed that Rac1 was located on the cytoplasmic side of the cell membrane, while P53 was located in the nucleus, suggesting a reciprocal influence (Supplementary Figure S1C). Interestingly, *rac1* and *p53* were up-regulated at the mRNA level upon SPM treatment, hinting at their roles in mediating the anti-OP effects of SPM (Figure 2I).

These findings emphasize the ability of SPM to activate osteogenesis and neuroprotection pathways while inhibiting bone resorption pathways in zebrafish larvae, again verifying its positive regulatory effects on osteoporotic bone homeostasis. Rac1 and P53 were also substantially increased after SPM intervention, suggesting potential roles in the anti-OP effect of SPM.

Rac1 inhibition impairs anti-OP effect of SPM

To investigate the contribution of Rac1 to the anti-OP effects of SPM, the Rac1 inhibitor 1A-116 was used based on the ability of SPM to enhance Rac1 expression (Figure 3A). Upon Rac1 suppression, the beneficial effects of SPM on mineralization almost disappeared (Figure 3B), accompanied by a decrease in osteoblast-related markers and an increase in osteoclast-related markers (Supplementary Figure S2A), suggesting that Rac1 may be a crucial molecule involved in mediating the effects of SPM on OP. Furthermore, as 1A-116 inhibited the expression of *sp7* in the maxillofacial bones of zebrafish larvae, the bone formation effects of SPM were dramatically weakened (Figure 3C). Further analysis showed that P53 expression and phosphorylation at the mRNA and protein level increased under SPM treatment, which was nullified post-Rac1 inhibition, indicating a role of Rac1 in regulating P53 expression (Figure 3D, E; Supplementary Figure S3). In summary, the amelioration of OP by SPM in zebrafish larvae is facilitated through the enhancement of Rac1 expression, with P53 potentially acting downstream of Rac1.

***Rac1* knockdown zebrafish larvae develop OP**

To further clarify the regulatory role of Rac1 on skeletal system development, CRISPRi technology was used for *rac1* gene knockdown (KD) in zebrafish embryos (Figure 3F, G). Results showed notably reduced notochord mineralization, down-regulation of osteoblast-related genes, and up-regulation of osteoclast-related genes in the KD larvae, suggesting OP onset (Figure 3H; Supplementary Figure S2B).

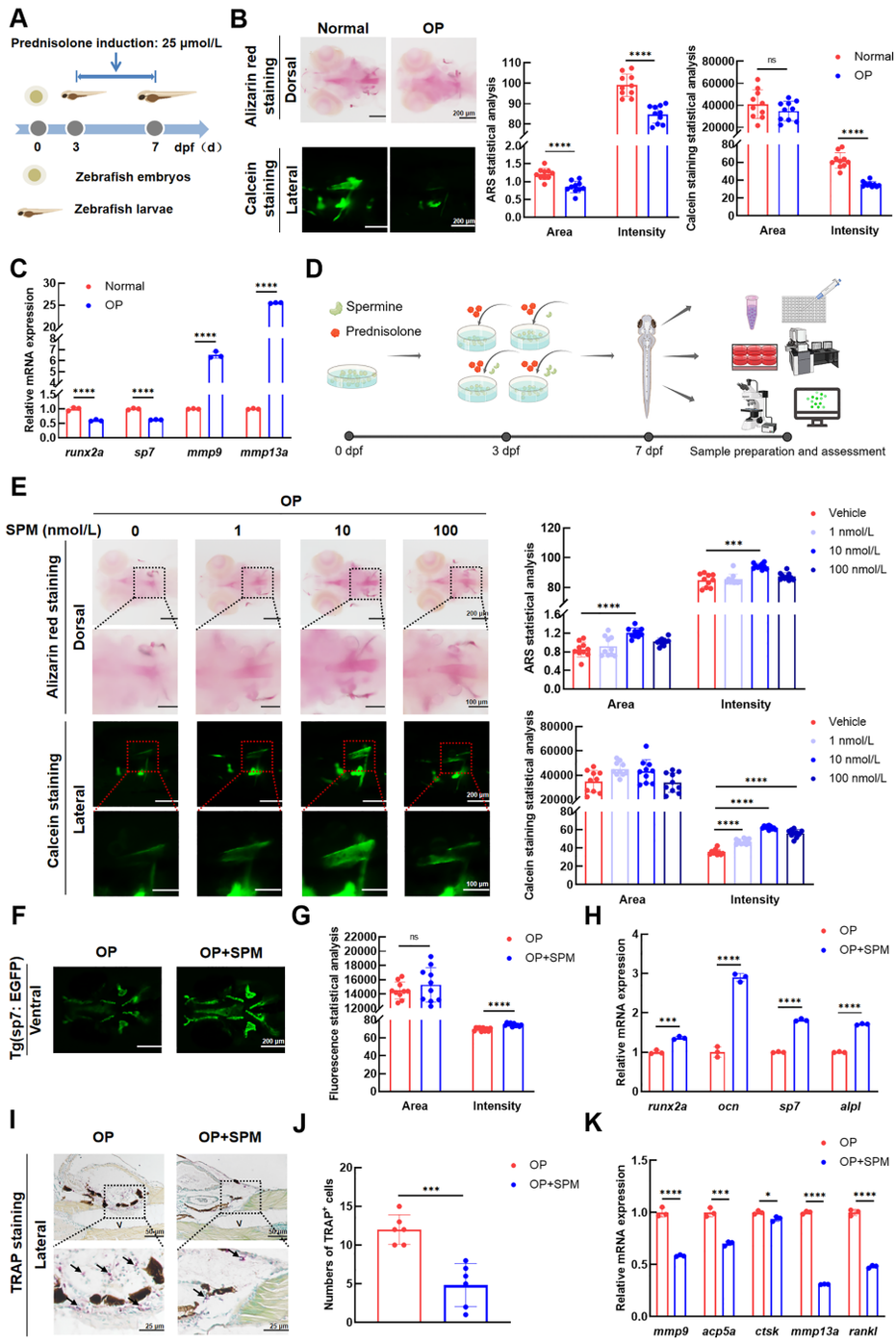

Figure 1 Spermine (SPM) alleviated prednisolone (PN)-induced osteoporosis (OP) in zebrafish larvae

A: Schematic of OP establishment in zebrafish larvae. Each group was established with three biological replicates, each replicate containing 30 larvae. B: Representative images of 7 dpf zebrafish larvae stained with alizarin red (upper panel) and calcein (lower panel). Scale bar: 200 μm. Statistical analysis of alizarin red staining (ARS) and calcein staining demonstrated the mineralized area and mean mineralized intensity at the notochord site of larvae (right panel, *n*=10). C: RT-qPCR results showed mRNA expression levels of genes related to osteoblasts (*runx2a*, *sp7*) and osteoclasts (*mmp9*, *mmp13a*) in the normal and OP groups. D: Experimental schematic of gradient concentrations of SPM (1 nmol/L, 10 nmol/L, 100 nmol/L) added to interfere with PN induction to measure its influence on bone homeostasis. Each group was established with three biological replicates, each replicate containing 30 larvae. E: Representative images of 7 dpf zebrafish larvae after ARS (upper panel) and calcein staining (lower panel). Scale bar: 200 μm for minor images; 100 μm for enlarged images. Statistical analysis indicated that 10 nmol/L SPM significantly improved bone formation and mineralization under OP conditions (right panel, *n*=10). F, G: Fluorescent images (scale bar: 200 μm) and quantitative analysis of OP and OP+SPM Tg (sp7: EGFP) zebrafish larvae in maxillofacial regions at 7 dpf (*n*=10). H: RT-qPCR results of osteoblast-related genes (*runx2a*, *ocn*, *sp7*, *alpl*) in OP and OP+SPM groups. I: TRAP staining of 7 dpf larvae in OP and OP+SPM groups. Scale bar: 50 μm for upper panel; 25 μm for lower panel. V: Vertebrae; Black arrows: Osteoclasts. J: TRAP-positive cell counting (*n*=6). K: RT-qPCR results of osteoclast-related genes (*mmp9*, *acp5a*, *ctsk*, *mmp13a*, *rankl*) in OP and OP+SPM groups. Results are presented as mean±SD. Statistical significance was determined using *t*-test for two groups and one-way analysis of variance (ANOVA) for multiple groups. ns: Not significant; *: $P<0.05$; **: $P<0.01$; ***: $P<0.001$; ****: $P<0.0001$.

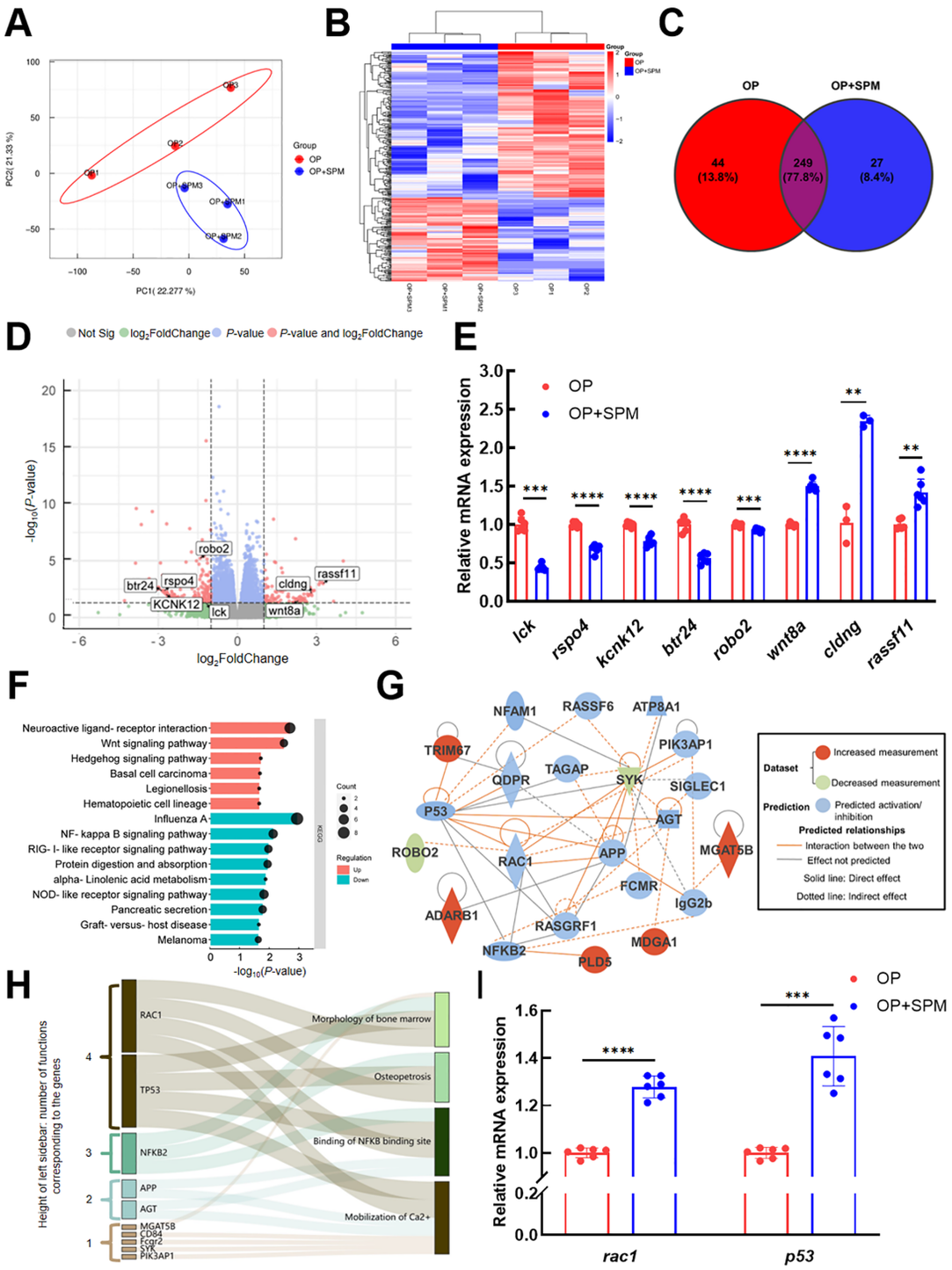

Figure 2 Possible mediating effects of Rac1 and P53 on anti-osteoporosis (OP) effects of spermine (SPM), as indicated by RNA-seq and IPA

A: Principal coordinate analysis (PCA) of zebrafish larvae at 7 dpf from OP and OP+SPM groups based on RNA-Seq. B: Hierarchical clustering heatmap compared to differentially expressed gene (DEG) levels between two groups. C: Venn diagram of distribution of all DEGs. D: Volcano plot of all detected genes based on RNA-seq, with significant DEGs ($\log_2|FC|\geq1$ and P-value≤0.05) highlighted in red. E: RT-qPCR was performed on selected DEGs to measure RNA-Seq accuracy. There were 20 larvae in each group for RNA extraction (n=20), and RT-qPCR was conducted three times. F: Histogram of KEGG enrichment analysis showing top pathways with the most significant changes (according to P-values). G: Potential molecular network predicted from DEG set using IPA. Red and green backgrounds represent up-regulated and down-regulated genes, respectively, while genes with blue backgrounds were predicted to change in the OP+SPM group compared with the OP group. H: Disease and functional analysis based on IPA. Selected diseases and functions related to bone metabolism and the skeletal system were matched with molecules in the network to determine their relationship. Results are represented using a Sankey chart. Colors on left sidebar indicate number of functions corresponding to the genes: brown, green, blue, and tan targeting four, three, two, and one function, respectively. I: *Rac1* and *p53* expression at mRNA level. There were 20 larvae in each group for RNA extraction (n=20), and RT-qPCR was conducted three times. Results are presented as mean±SD. Statistical significance was determined by t-test with *: P<0.05; **: P<0.01; ***: P<0.001; ****: P<0.0001.

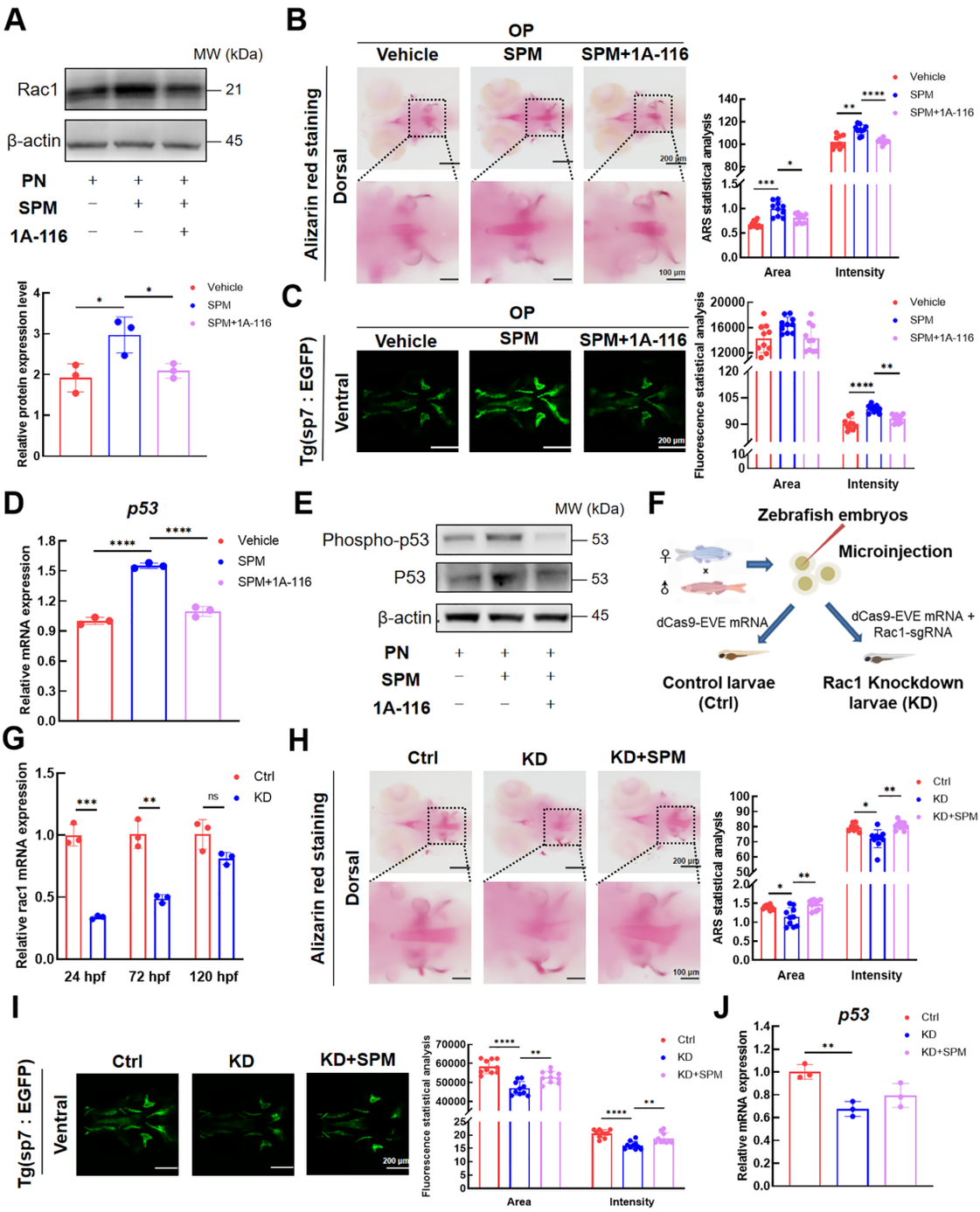

Figure 3 Spermine (SPM) enhanced osteogenesis in zebrafish larvae via Rac1 up-regulation, while Rac1 knockdown induced osteoporosis

A–E: Zebrafish experiments with Rac1 inhibitor 1A-116. A: SPM increased Rac1 protein expression in larvae receiving PN+SPM (SPM group) compared to larvae receiving PN (Vehicle group), while 1A-116 inhibited Rac1 protein expression in larvae receiving PN+SPM+1A-116 (SPM+1A-116 group). B: ARS results from 7 dpf larvae in the same groups as shown in Figure 3A (n=10). Scale bar: 200 μm for upper panel; 100 μm for lower panel. C: Representative fluorescent images and quantitative analysis of 7 dpf Tg (sp7: EGFP) zebrafish larvae in maxillofacial regions in the Vehicle, SPM, and SPM+1A-116 groups (scale bar: 200 μm, n=10). D: RT-qPCR results showing up-regulation of *p53* expression in OP+SPM group, which was reversed by 1A-116. E: Western blotting analysis of P53 and Phospho-p53 proteins in zebrafish larvae at day 7. F–J: *Rac1* knockdown experiments in zebrafish. F: Schematic of CRISPRi microinjection. Mixed dCas9-EVE mRNA and *rac1*-sgRNAs were microinjected into zebrafish embryos within half an hour after collection. *Rac1* knockdown (KD) group, SPM intervention (KD+SPM) group, and control (Ctrl) group microinjected with dCas9-EVE mRNA. Ctrl and KD groups grew and developed normally, while the KD+SPM group were subjected to SPM intervention on days 3–7. All samples were collected on day 7. G: *Rac1* knockdown efficiency was verified. H: ARS results of 7 dpf larvae in the Ctrl, KD, and KD+SPM groups (n=10). Scale bar: 200 μm for upper panel; 100 μm for lower panel. I: Representative fluorescent images and quantitative analysis of 7 dpf Tg (sp7: EGFP) zebrafish larvae in maxillofacial regions in the Ctrl, KD, and KD+SPM groups (scale bar: 200 μm, n=10). J: RT-qPCR results showing *p53* expression in the Ctrl, KD, and KD+SPM groups. Results are presented as mean±SD. Statistical significance was determined by *t*-test for two groups and one-way ANOVA for multiple groups. ns: Not significant; *: P<0.05; **: P<0.01; ***: P<0.001; ****: P<0.0001.

SPM markedly alleviated these abnormalities by increasing notochord mineralization and promoting *sp7* expression in the maxillofacial bones of KD larvae (Figure 3H, I). Furthermore, results showed down-regulation of *p53* after *rac1* knockdown and partial rebound after SPM intervention, further highlighting the regulatory role of Rac1 on P53 expression (Figure 3J). Taken together, these findings indicate that *rac1* knockdown results in OP in zebrafish larvae, suggesting that Rac1 may be an effective target for anti-OP therapy.

SPM reduces PN toxicity induced in zebrafish embryos and ameliorates disturbed behavior of zebrafish larvae

In screening new drugs for diseases, it is essential to evaluate drug safety alongside drug effectiveness. Therefore, we selected zebrafish embryos to measure the biosafety of SPM, as shown in Figure 4A. SPM showed no significant adverse effects on the morphogenesis, survival, or malformation of embryos under both normal and PN-induced conditions (Figure 4B–D). Furthermore, while early PN intervention reduced embryonic autonomous movements (24 hpf) and heart rate (48 hpf), indicating adverse effects on embryo development, SPM treatment was associated with increased embryonic autonomous movements and a normalization of heart rate (Figure 4E). These findings indicate that SPM exhibits high biosafety and can reduce early neurotoxicity and cardiotoxicity induced by PN.

Considering its protective effects on embryonic neural development in zebrafish and ability to activate the neuroactive ligand-receptor interaction signaling pathway (Figure 2F), we further evaluated the impact of SPM on nervous system development in zebrafish larvae through behavioral testing (Figure 4F). Analysis of movement patterns and heatmaps revealed that larvae in the OP group displayed more restricted movement, seldom venturing into the central area, whereas the trajectories of the OP+SPM larvae showed similarities to those observed in the normal group (Figure 4G). Metrics of speed and distance demonstrated that the OP+SPM larvae moved at significantly higher speeds and covered greater distances compared to those in the OP group, surpassing even the activity levels of the normal group, indicating a marked improvement in larval behavior following SPM administration (Figure 4H, I). Additionally, larvae in both the normal and OP+SPM groups displayed bolder exploration, as evidenced by their reduced average distance from the center (Figure 4J). Analysis of motility states further indicated increased activity in larvae following treatment with SPM (Figure 4K). In general, these results emphasize the role of SPM in enhancing nervous system development in zebrafish larvae affected by OP.

SPM shows excellent potential to strengthen bone development and mineralization

We identified the regulatory effects of SPM on bone homeostasis in zebrafish with OP and the key molecules mediating its effects. However, whether SPM can affect the developmental processes and mineralization of the skeletal system under normal conditions is still unknown. Therefore, we first conducted experiments on normal zebrafish larvae and found that SPM facilitated mean mineralization intensity in the notochord site and enhanced *sp7* expression in the maxillofacial bones of larvae, thus significantly promoting bone formation and mineralization (Figure 5A–D).

To further assess the effects of SPM on the skeletal system under normal physiological conditions, we also carried out experiments on mice (Figure 5E). Notably, SPM administration for three consecutive weeks promoted an increase in tibial BMD in mice (Figure 5F). Micro-CT showed that the trabecular bone structure of the femur in the SPM group was more compact, characterized by increased trabecular bone thickness (Tb.Th) and decreased degree of separation (Tb.Sp) (Figure 5G, H). H&E staining also indicated that the SPM group had an increased number of bone trabeculae and presented with a thicker structure (Figure 5I). Quantitative statistical analysis of bone trabeculae below the epiphysis cartilage region also verified a more significant trabecular bone area in the SPM group, consistent with the micro-CT results (Figure 5J). These findings confirmed that SPM displays a satisfactory osteogenic effect in both zebrafish larvae and mice, highlighting its potential as an alternative bone-strengthening agent in the future.

DISCUSSION

OP represents a major public health issue due to its wide prevalence and the significant side effects associated with current drug therapies, emphasizing the urgency for novel therapeutic approaches. Metabolite-based therapies have emerged as a promising treatment for bone health in research on novel OP treatments (Lucas et al., 2018; Montalvany-Antonucci et al., 2019; Quach & Britton, 2017; Zaiss et al., 2019). Given their endogenous nature, these metabolites offer several advantages in terms of fewer adverse reactions over prolonged periods compared to traditional synthetic drugs, highlighting their effectiveness and biosafety. In the current study, we specifically explored the anti-OP properties of the metabolite SPM, a polyamine known for its extensive biological functions across various organisms and for its potential in OP management (Chevalier et al., 2020; Yamamoto et al., 2012). Despite evidence supporting the utility of SPM in OP, its impacts on bone metabolism and precise mechanisms of action remain inconclusive.

Hence, we explored the effects of SPM on osteoporotic bone homeostasis based on a zebrafish model of glucocorticoid-induced OP (GIOP). Compared to rodents, zebrafish offer unique drug development and testing advantages, facilitating a broader understanding of drug impacts. As our knowledge of their bone development has expanded, zebrafish have been increasingly used to study bone-related diseases (Chen et al., 2017; Fleming et al., 2005) and screen novel anti-OP drugs (Lin et al., 2022; Qiu et al., 2023; Wang et al., 2018, 2023; Yin et al., 2019; Zhong et al., 2023), significantly enhancing research efficiency and reducing costs.

Our findings revealed that SPM administration strengthened notochord mineralization in zebrafish larvae with OP by facilitating bone formation and inhibiting bone resorption, while maintaining excellent biosafety. These results not only elucidate the beneficial regulatory role of SPM on osteoporotic bone homeostasis but further demonstrate the capacity of endogenous metabolites to influence bone metabolism.

The zebrafish *rac1* gene, also known as *rac1a*, belongs to the Rac family of small GTPases and plays a vital role in a variety of cellular processes, including cytoskeletal assembly (Ding et al., 2022), cell development (Tejada-Simon, 2015), DNA damage reparation (Fritz & Henninger, 2015), cell motility, and migration (Chan et al., 2005), and has thus become an attractive anti-tumor target (Bailly et al., 2022; Ma et al., 2023). During osteoclast differentiation, Rac1 is highly

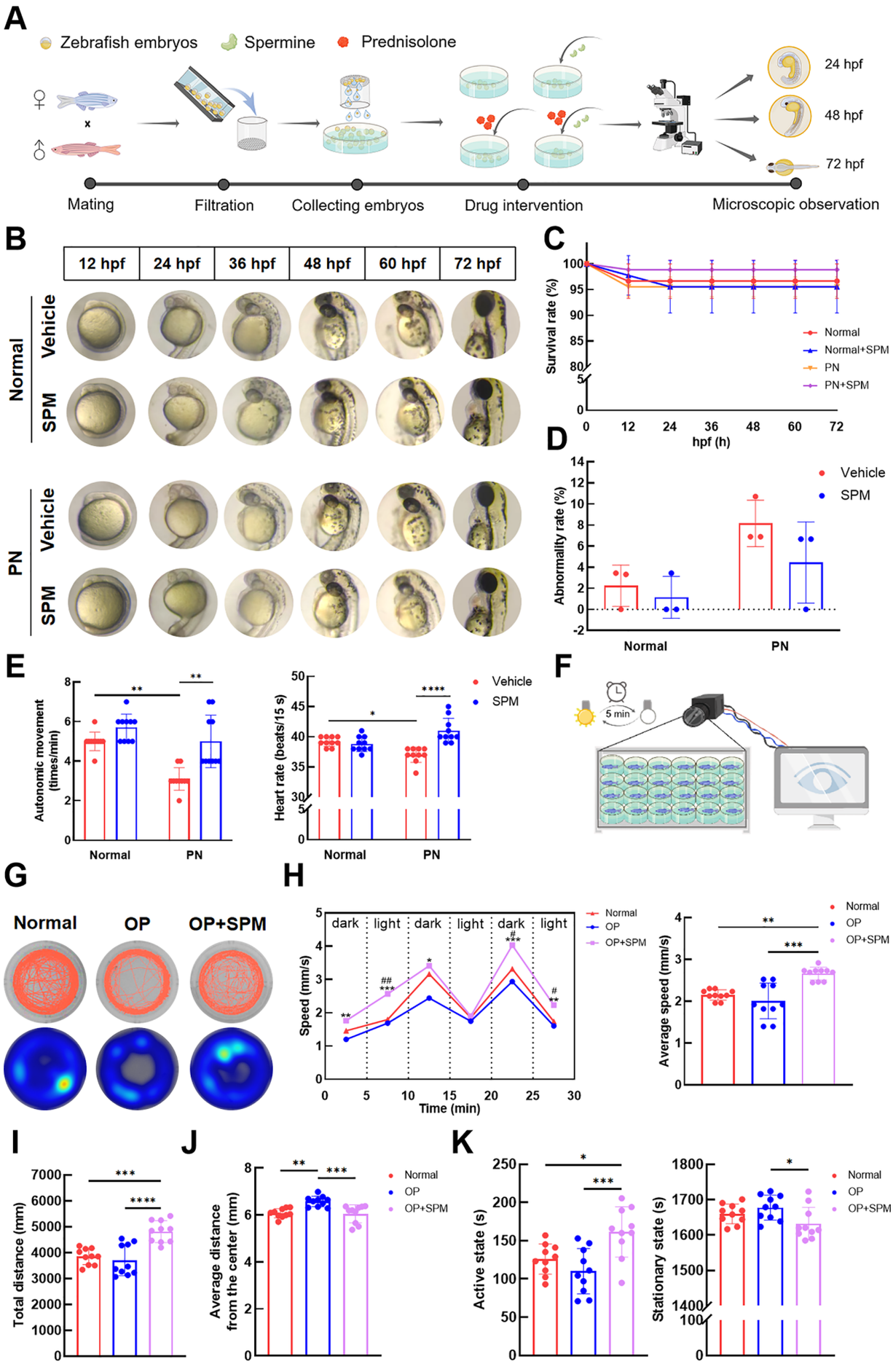
A
Zebrafish embryos
Spermine
Prednisolone
24 hpf
48 hpf
72 hpf
Mating
Filtration
Collecting embryos
Drug intervention
Microscopic observation
B
12 hpf
24 hpf
36 hpf
48 hpf
60 hpf
72 hpf
Normal
Vehicle
SPM
PN
Vehicle
SPM
C
Survival rate (%)
hpf (h)
Normal
Normal+SPM
PN
PN+SPM
D
Abnormality rate (%)
Vehicle
SPM
Normal
PN
E
Autonomic movement (times/min)
Heart rate (beats/15 s)
Vehicle
SPM
Normal
PN
F
5 min
G
Normal
OP
OP+SPM
H
dark
light
dark
light
dark
light
Speed (mm/s)
Time (min)
Normal
OP
OP+SPM
Average speed (mm/s)
I
Total distance (mm)
J
Average distance from the center (mm)
K
Active state (s)
Stationary state (s)

Figure 4 Spermine (SPM) exhibited excellent biosafety and exerted neuroprotective effects in zebrafish to a certain extent

A–E: Early embryonic development experiments of zebrafish were conducted to assess the biosafety of SPM in normal conditions and PN induction. A: Schematic of experimental design. All embryos were divided into four groups: Normal+Vehicle, Normal+SPM, PN+Vehicle, and PN+SPM. Each group was established with three biological replicates, each replicate containing 30 embryos. B: Representative images of embryos at different time points (12 hpf, 24 hpf, 36 hpf, 48 hpf, 60 hpf, 72 hpf). C: Statistical analysis of embryo survival rate at different time points (0 hpf, 12 hpf, 24 hpf, 36 hpf, 48 hpf, 60 hpf, 72 hpf). D: Statistical analysis of embryo abnormality rate at 72 hpf. E: Statistical results of embryo autonomous movement frequency at 24 hpf and heartbeat within 15 s at 48 hpf (n=10). F–K: Behavioral tests on 7 dpf zebrafish larvae in Normal, OP, and OP+SPM groups were conducted to observe the effect of SPM on neural tissue. F: Schematic of experimental design. G: Representative heatmaps and trajectory plots of larvae. H: Average swimming speed of larvae in each period (left panel) and average speed within 30 min (right panel). *: Significant difference between OP and OP+SPM groups (n=10, *: P<0.05; **: P<0.01; ***: P<0.001.). $^{\#}$: Significant difference between Normal and OP+SPM groups ($^{\#}$: P<0.05; $^{\#\#}$: P<0.01). I: Statistical analysis of total swimming distance in 30 min (n=10). J: Statistical analysis of average distance from the center over 30 min in each group (n=10). K: Activity state analysis of larvae (n=10). Results are presented as mean±SD. Statistical significance was determined by t-test for two groups and one-way ANOVA for multiple groups. ns: Not significant; *: P<0.05; **: P<0.01; ***: P<0.001; ****: P<0.0001.

up-regulated (Zhang et al., 2022; Zhou et al., 2020) and thought to be involved in mediating the inhibition of osteoclast differentiation (Guo et al., 2021), although other studies have reported different results (Li et al., 2023a). Rac1 is also necessary for normal osteogenic function and bone mineral density maintenance (Huck et al., 2020). Many studies have explored the influence of Rac1 on bone metabolism, with most suggesting that Rac1 is a potent target for the treatment of primary OP characterized by hyperactive osteoclastic resorption (He et al., 2016; Kim et al., 2009; Magalhaes et al., 2011; Yan et al., 2008). In contrast, the role of Rac1 on bone homeostasis in GIOP has rarely been reported. Some studies have suggested that imbalance or abnormal function of Rac1 will negatively impact the skeletal system, regardless of whether it is up-regulated or down-regulated (Chen et al., 2021; Mäkitie et al., 2021). In this study, SPM induced the expression of Rac1, suppressing bone resorption and facilitating bone formation. Intervention with the Rac1 inhibitor resulted in the almost complete disappearance of the anti-OP effect of SPM, strongly indicating the significant role of Rac1 in this process.

We hypothesized that the defining characteristic of GIOP is a sustained decrease in bone formation, accompanied by an initial temporary increase in bone resorption (Buckley & Humphrey, 2018), suggesting that Rac1 may play a dominant role in accelerating bone formation and inhibiting bone resorption. Observations indicated that SPM restored Rac1 expression to baseline levels, rather than leading to its overexpression, implying that maintaining Rac1 homeostasis is conducive to positively regulating bone metabolism in the skeletal system. Remarkably, *rac1* knockdown zebrafish larvae showed phenotypes consistent with those observed with the inhibitor, suggesting that Rac1 strongly impacts bone formation and mineralization. This study clarified the molecular mechanism by which SPM influences osteoporotic bone homeostasis, addressing a gap in our understanding of the role of Rac1 in bone formation and suggesting Rac1 as a potential therapeutic target for GIOP, although further investigation into its specific activation mechanisms is warranted.

Identified through RNA-Seq and IPA as a potentially effective molecule, changes in P53 were also measured in this study. The results showed that SPM had a dual effect by promoting both P53 expression and phosphorylation, while simultaneously inhibiting Rac1, thereby reversing the effect of SPM on P53 expression and phosphorylation. These results suggest that P53 is a potential downstream molecule of Rac1, with SPM promoting the expression of both, consistent with previous researches (Mishra et al., 2019; Soliman et al., 2021).

In addition to skeletal effects, we further evaluated the impact of SPM on the nervous system of zebrafish embryos and larvae based on KEGG enrichment analysis and behavioral testing. The neuroprotective effects of SPM were confirmed based on improvements in glucocorticoid-induced embryonic neurotoxicity in embryos and behavioral abnormalities in zebrafish larvae. Prior to this investigation, the influence of SPM on the nervous system was largely unknown. Studies have indicated that macrophages express high levels of SPM during spinal cord repair within intercostal nerve grafts (Kuo et al., 2007) and that SPM protects nerve tissue in rats with acute cerebral ischemia-reperfusion injury (ACIR) (Du et al., 2017). Our study highlighted the effects of SPM on the nervous system in zebrafish, providing additional evidence for its positive neuroprotective function. However, further research is needed to elucidate the complete role of SPM in neural development and homeostasis.

Amid the evolving landscape of health economics, there is a perceptible shift in therapeutic strategies from merely treating existing diseases to preventing diseases. This paradigm shift is particularly evident in contemporary medical research (Sato et al., 2022), indicating that drugs are no longer limited to therapeutic applications but also to disease prevention. SK-124, identified for its anti-OP potential, has been shown to increase osteoblast numbers and trabecular bone mass in healthy mice without inducing short-term toxicity, illustrating potential preventive effects on the occurrence of OP (Sato et al., 2022). Similarly, ursodeoxycholic acid (UDCA) has been shown to halt disease progression, improve prognosis in COVID-19 patients, and provide benefits to healthy subjects (Brevini et al., 2023). In the current study, we evaluated the effects of SPM on the skeletal system of PN-induced and healthy zebrafish larvae and mice, revealing its favorable role in promoting bone formation and mineralization across both models. These empirical insights offer a fresh perspective on OP prevention, suggesting that SPM may be a bone-fortifying agent akin to the ubiquitously consumed calcium tablets.

In summary, our results suggest that SPM, mediated by the Rac1-P53 axis, holds promise as a potential anti-OP drug with evident biosafety and neuroprotective attributes (Figure 6). Moreover, the potential of SPM to bolster bone health under normal conditions suggests its prospective use as a daily supplement. This work broadens our understanding of the interactions between SPM and the skeletal system and provides a foundation for innovative OP treatments.

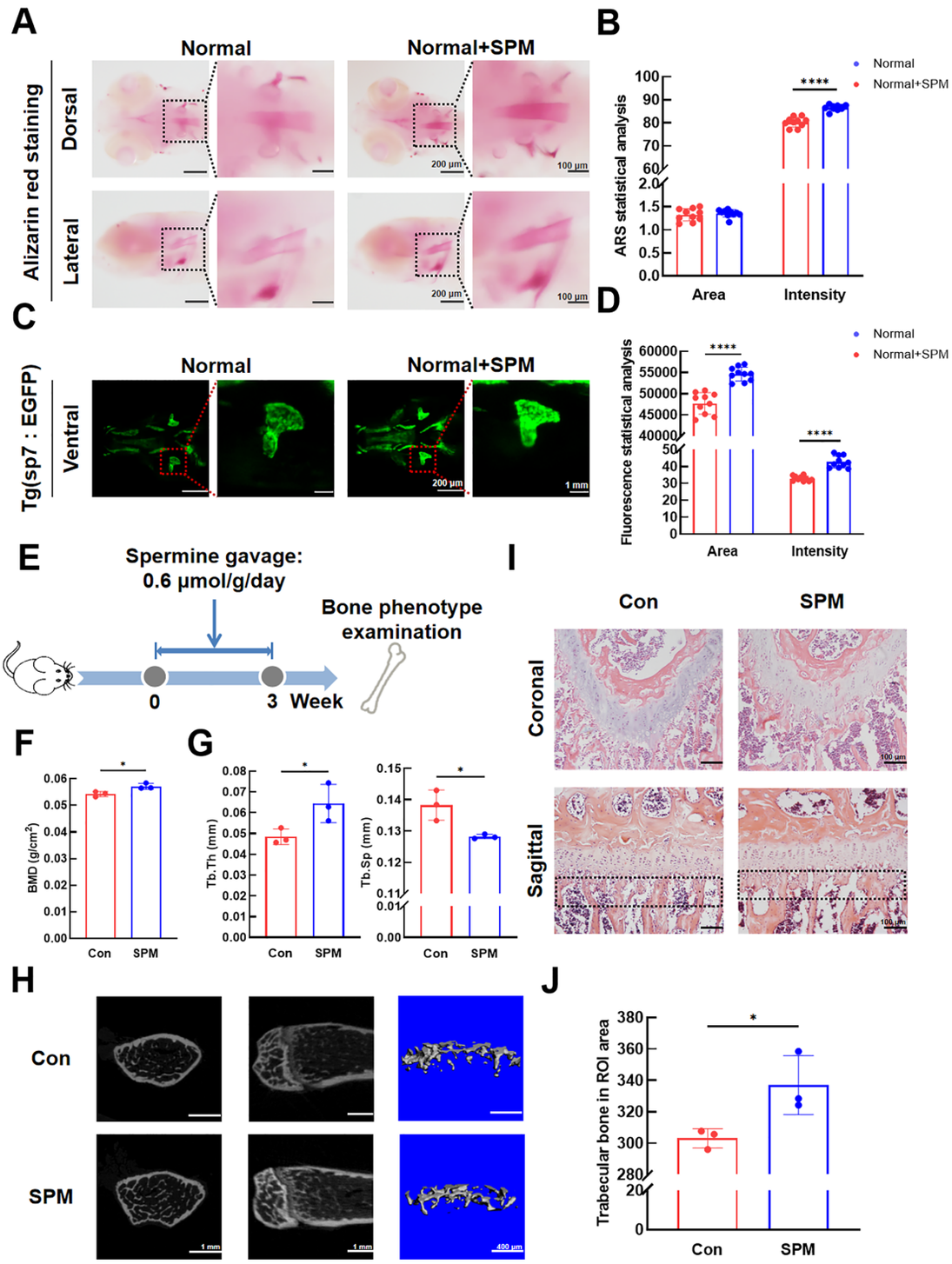

Figure 5 Spermine (SPM) showed osteogenic effects on healthy zebrafish and mice

A–D: Zebrafish experiments. Healthy zebrafish larvae were administered SPM from 3 to 7 dpf. Each group was established with three biological replicates, each replicate containing 30 larvae. A, B: ARS results of healthy larvae (Normal group) and larvae receiving SPM (Normal+SPM group) on day 7 (n=10). Scale bar: 200 μm for small images; 100 μm for enlarged images. C, D: Representative fluorescent images and quantitative analysis of 7 dpf Tg (sp7: EGFP) zebrafish larvae in maxillofacial regions in Normal and Normal+SPM groups (n=10). Scale bar: 200 μm for small images; 1 mm for enlarged images. E–J: Mouse experiments exploring effects of SPM on skeletal system. E: Schematic of experimental design. After one week of acclimatization, 7-week-old mice were chosen, each group consisting of three replicates. Mice in the SPM group were gavaged with SPM at a dose of 0.6 μmol/g/d, and mice in the Con group were gavaged with equal volume saline as a control. Gavage continued for three weeks, after which the mice were sacrificed to detect skeletal system phenotypes. F: BMD scanning results (n=3). G: Micro-CT analysis of bone trabecular within femurs (n=3). Scale bars for left, middle, and right panels are 1 mm, 1 mm, and 400 μm, respectively. H: Representative micro-CT images of trabecular bone below the growth plate of femurs from 10-week-old mice in the Con and SPM groups. I: H&E staining images of histological sections of femur. Scale bar: 200 μm for upper panel: 100 μm for lower panel. J: Trabecular bone area in black box area in Figure 5I (ROI) was analyzed using ImageJ (n=3). Results are presented as mean±SD. Statistical significance was determined by t-test. ns: Not significant; *: P<0.05; **: P<0.01; ***: P<0.001; ****: P<0.0001.

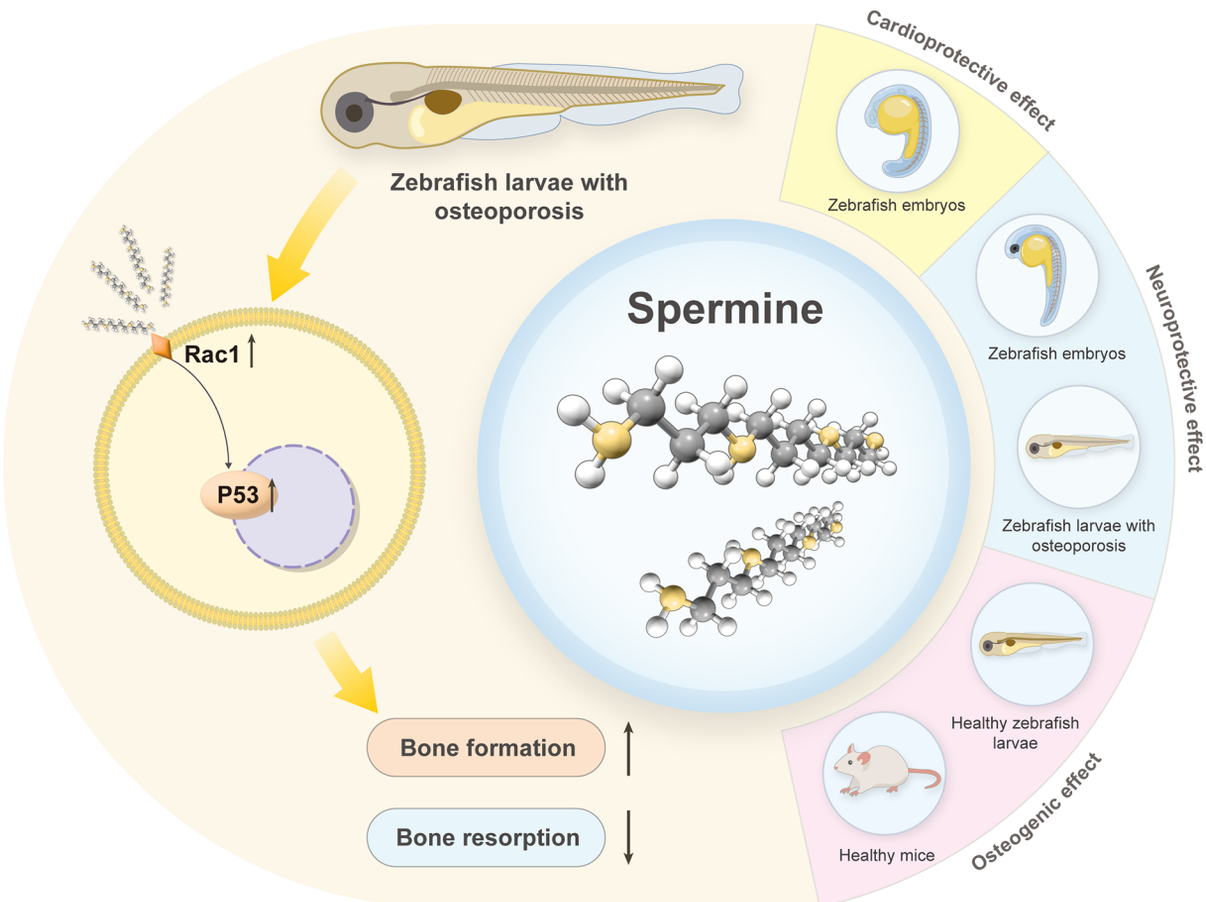

Figure 6 Summary overview

Spermine (SPM) improved osteoporosis (OP) in zebrafish larvae via the Rac1-P53 axis, showing cardioprotective and neuroprotective effects. Under normal conditions, SPM also promoted bone formation and mineralization in mice and zebrafish, suggesting an osteogenic effect.

DATA AVAILABILITY

The sequencing raw data reported in this paper have been deposited in the National Center for Biotechnology Information database (PRJNA1065252), Genome Sequence Archive (GSA: CRA014465), and Science Data Bank database (DOI: 10.57760/sciencedb.j00139.00106).

SUPPLEMENTARY DATA

Supplementary data to this article can be found online.

COMPETING INTERESTS

The authors declare that they have no competing interests.

AUTHORS' CONTRIBUTIONS

R.X.J. designed the study, conducted the experiments, and drafted the initial manuscript; N.H. played a significant role in developing the methodology and creating animal models; Y.W.D. and H.G. performed the data analysis; L.W.H. and N.L. contributed to the results verification; J.W. conceived the study and critically revised the manuscript; X.Q.J. supervised the study and revised the manuscript. All authors read and approved the final version of the manuscript.

ACKNOWLEDGMENTS

We sincerely appreciate the assistance with the IPA system provided by Wen-Jing Ding from the Library of Shanghai Jiao Tong University School of Medicine for this study. We thank Xiang Gao (Neo Biology Company, Shanghai) for providing RNA-Seq technical support.

REFERENCES

Abtahi S, Driessen JHM, Vestergaard P, et al. 2018. RETRACTED ARTICLE: Secular trends in major osteoporotic fractures among 50+ adults in Denmark between 1995 and 2010. *Archives of Osteoporosis*, **13**(1): 91.

Bailly C, Beignet J, Loirand G, et al. 2022. Rac1 as a therapeutic anticancer target: Promises and limitations. *Biochemical Pharmacology*, **203**: 115180.

Barrett R, Chappell C, Quick M, et al. 2006. A rapid, high content, *in vivo* model of glucocorticoid-induced osteoporosis. *Biotechnology Journal*, **1**(6): 651−655.

Black DM, Cummings SR, Karpf DB, et al. 1996. Randomised trial of effect of alendronate on risk of fracture in women with existing vertebral fractures. *The Lancet*, **348**(9041): 1535−1541.

Brevini T, Maes M, Webb GJ, et al. 2023. FXR inhibition may protect from SARS-CoV-2 infection by reducing ACE2. *Nature*, **615**(7950): 134−142.

Buckley L, Humphrey MB. 2018. Glucocorticoid-induced osteoporosis. *New England Journal of Medicine*, **379**(26): 2547−2556.

Cao W, Wu XJ, Jia G, et al. 2017. New insights into the role of dietary spermine on inflammation, immune function and related-signalling molecules in the thymus and spleen of piglets. *Archives of Animal Nutrition*, **71**(3): 175−191.

Chan AY, Coniglio SJ, Chuang YY, et al. 2005. Roles of the Rac1 and Rac3 GTPases in human tumor cell invasion. *Oncogene*, **24**(53): 7821−7829.

Chen C, Zheng YL, Li X, et al. 2022. Cysteamine affects skeletal development and impairs motor behavior in zebrafish. *Frontiers in Pharmacology*, **13**: 966710.

Chen JR, Lai YH, Tsai JJ, et al. 2017. Live fluorescent staining platform for drug-screening and mechanism-analysis in zebrafish for bone mineralization. *Molecules*, **22**(12): 2068.

Chen X, Zhu WW, Xu RY, et al. 2021. Geranylgeraniol restores zoledronic acid-induced efferocytosis inhibition in bisphosphonate-related

osteonecrosis of the jaw. *Frontiers in Cell and Developmental Biology*, **9**: 770899.

Chen ZJ, Song ZY, Yang JJ, et al. 2019. *Sp7/osterix* positively regulates *dlx2b* and *bglap* to affect tooth development and bone mineralization in zebrafish larvae. *Journal of Biosciences*, **44**(6): 127.

Chevalier C, Kieser S, Çolakoğlu M, et al. 2020. Warmth prevents bone loss through the gut microbiota. *Cell Metabolism*, **32**(4): 575−590.e7.

Das UN. 2021. Bioactive lipids in COVID-19-further evidence. *Archives of Medical Research*, **52**(1): 107−120.

Dietrich K, Fiedler IAK, Kurzyukova A, et al. 2021. Skeletal biology and disease modeling in zebrafish. *Journal of Bone and Mineral Research*, **36**(3): 436−458.

Ding BJ, Yang S, Schaks M, et al. 2022. Structures reveal a key mechanism of WAVE regulatory complex activation by Rac1 GTPase. *Nature Communications*, **13**(1): 5444.

Du H, Ming X, Zhou SK. 2017. Pre-treatment with spermine for acute cerebral ischemia/reperfusion injuries. *Experimental and Therapeutic Medicine*, **14**(1): 169−172.

Fleming A, Sato M, Goldsmith P. 2005. High-throughput in vivo screening for bone anabolic compounds with zebrafish. *SLAS Discovery*, **10**(8): 823−831.

Fritz G, Henninger C. 2015. Rho GTPases: novel players in the regulation of the DNA damage response?. *Biomolecules*, **5**(4): 2417−2434.

Gopinath V. 2023. Osteoporosis. *Medical Clinics of North America*, **107**(2): 213−225.

Guo Q, Kang HL, Wang J, et al. 2021. Inhibition of ACLY leads to suppression of osteoclast differentiation and function via regulation of histone acetylation. *Journal of Bone and Mineral Research*, **36**(10): 2065−2080.

Guo WM, Jin P, Li RM, et al. 2023. Dynamic network biomarker identifies *cdkn1a*-mediated bone mineralization in the triggering phase of osteoporosis. *Experimental & Molecular Medicine*, **55**(1): 81−94.

He H, Cao SL, Niu TH, et al. 2016. Network-based meta-analyses of associations of multiple gene expression profiles with bone mineral density variations in women. *PLoS One*, **11**(1): e0147475.

He HL, Wang CQ, Tang QF, et al. 2018. Possible mechanisms of prednisolone-induced osteoporosis in zebrafish larva. *Biomedicine & Pharmacotherapy*, **101**: 981−987.

Huang HX, Lin H, Lan F, et al. 2018. Application of bone transgenic zebrafish in anti-osteoporosis chemical screening. *Animal Models and Experimental Medicine*, **1**(1): 53−61.

Huck K, Sens C, Wuerfel C, et al. 2020. The rho GTPase RAC1 in osteoblasts controls their function. *International Journal of Molecular Sciences*, **21**(2): 385.

Iezaki T, Hinoi E, Yamamoto T, et al. 2012. Amelioration by the natural polyamine spermine of cartilage and bone destruction in rats with collagen-induced arthritis. *Journal of Pharmacological Sciences*, **119**(1): 107−111.

Jiang JT, Wang WW, Sun F, et al. 2021a. Bacterial infection reinforces host metabolic flux from arginine to spermine for NLRP3 inflammasome evasion. *Cell Reports*, **34**(10): 108832.

Jiang Y, Xin N, Yang J, et al. 2021b. Prednisolone suppresses collagen-encoding gene expression causing cartilage defects in zebrafish larvae. *Environmental Toxicology and Pharmacology*, **87**: 103719.

Kellier-Steele N, Casso D, Anderson A, et al. 2022. Assessing the incidence of osteosarcoma among teriparatide-treated patients using linkage of commercial pharmacy and state cancer registry data, contributing to the removal of boxed warning and other labeling changes. *Bone*, **160**: 116394.

Kemmak AR, Rezapour A, Jahangiri R, et al. 2020. Economic burden of osteoporosis in the world: A systematic review. *Medical Journal of the Islamic Republic of Iran*, **34**: 154.

Kim H, Choi HK, Shin JH, et al. 2009. Selective inhibition of RANK blocks osteoclast maturation and function and prevents bone loss in mice. *Journal of Clinical Investigation*, **119**(4): 813−825.

Kim SH, Lee YK, Kim TY, et al. 2021. Incidence of and risk for osteonecrosis of the jaw in Korean osteoporosis patients treated with bisphosphonates: A nationwide cohort-study. *Bone*, **143**: 115650.

Krege JH, Gilsenan AW, Komacko JL, et al. 2022. Teriparatide and osteosarcoma risk: history, science, elimination of boxed warning, and other label updates. *JBMR Plus*, **6**(9): e10665.

Kuo HS, Tsai MJ, Huang MC, et al. 2007. The combination of peripheral nerve grafts and acidic fibroblast growth factor enhances arginase I and polyamine spermine expression in transected rat spinal cords. *Biochemical and Biophysical Research Communications*, **357**(1): 1−7.

Li Q, Yue T, Du XY, et al. 2023a. HSC70 mediated autophagic degradation of oxidized PRL2 is responsible for osteoclastogenesis and inflammatory bone destruction. *Cell Death & Differentiation*, **30**(3): 647−659.

Li X, Li F, Ye F, et al. 2023b. Spermine is a natural suppressor of AR signaling in castration-resistant prostate cancer. *Cell Reports*, **42**(7): 112798.

Lin WY, Dharini KK, Peng CH, et al. 2022. Zebrafish models for glucocorticoid-induced osteoporosis. *Tzu Chi Medical Journal*, **34**(4): 373−380.

Lucas S, Omata Y, Hofmann J, et al. 2018. Short-chain fatty acids regulate systemic bone mass and protect from pathological bone loss. *Nature Communications*, **9**(1): 55.

Ma N, Xu EQ, Luo Q, et al. 2023. Rac1: a regulator of cell migration and a potential target for cancer therapy. *Molecules*, **28**(7): 2976.

MacRae CA, Peterson RT. 2015. Zebrafish as tools for drug discovery. *Nature Reviews Drug Discovery*, **14**(10): 721−731.

Magalhaes JKRS, Grynpas MD, Willett TL, et al. 2011. Deleting Rac1 improves vertebral bone quality and resistance to fracture in a murine ovariectomy model. *Osteoporosis International*, **22**(5): 1481−1492.

Mäkitie RE, Henning P, Jiu YM, et al. 2021. An *ARHGAP25* variant links aberrant Rac1 function to early-onset skeletal fragility. *JBMR Plus*, **5**(7): e10509.

Mishra M, Duraisamy AJ, Bhattacharjee S, et al. 2019. Adaptor protein p66Shc: a link between cytosolic and mitochondrial dysfunction in the development of diabetic retinopathy. *Antioxidants & Redox Signaling*, **30**(13): 1621−1634.

Montalvany-Antonucci CC, Duffles LF, De Arruda JAA, et al. 2019. Short-chain fatty acids and FFAR2 as suppressors of bone resorption. *Bone*, **125**: 112−121.

Niu PF, Zhong ZM, Wang MY, et al. 2017. Zinc finger transcription factor Sp7/Osterix acts on bone formation and regulates *col10a1a* expression in zebrafish. *Science Bulletin*, **62**(3): 174−184.

Pegg AE. 2014. The function of spermine. *IUBMB Life*, **66**(1): 8−18.

Peng CH, Lin WY, Li CY, et al. 2022. Gu Sui Bu (*Drynaria fortunei* J. Sm.) antagonizes glucocorticoid-induced mineralization reduction in zebrafish larvae by modulating the activity of osteoblasts and osteoclasts. *Journal of Ethnopharmacology*, **297**: 115565.

Pucciarelli S, Moreschini B, Micozzi D, et al. 2012. Spermidine and spermine are enriched in whole blood of Nona/centenarians. *Rejuvenation Research*, **15**(6): 590−595.

Qiu Y, Ying JY, Yan FJ, et al. 2023. Novel antiosteoporotic peptides purified from protein hydrolysates of taihe black-boned silky fowl: By larval zebrafish model and molecular docking. *Food Research International*, **169**: 112850.

Quach D, Britton RA. 2017. Gut microbiota and bone health. *Advances in Experimental Medicine and Biology*, **1033**: 47−58.

Sadasivan SK, Vasamsetti B, Singh J, et al. 2014. Exogenous administration of spermine improves glucose utilization and decreases bodyweight in mice. *European Journal of Pharmacology*, **729**: 94−99.

Sagar NA, Tarafdar S, Agarwal S, et al. 2021. Polyamines: functions,

metabolism, and role in human disease management. *Medical Sciences*, **9**(2): 44.

Sato T, Andrade CDC, Yoon SH, et al. 2022. Structure-based design of selective, orally available salt-inducible kinase inhibitors that stimulate bone formation in mice. *Proceedings of the National Academy of Sciences of the United States of America*, **119**(50): e2214396119.

Soliman NA, El Gheit REA, Ghafar MTA, et al. 2021. Unraveling the biomechanistic role of Rac1/TWEAK/Fn14/NF-κB intricate network in experimentally doxorubicin-induced cardiotoxicity in rats: The role of curcumin. *Journal of Biochemical and Molecular Toxicology*, **35**(8): e22829.

Tejada-Simon MV. 2015. Modulation of actin dynamics by Rac1 to target cognitive function. *Journal of Neurochemistry*, **133**(6): 767−779.

Vrijsen S, Besora-Casals L, Van Veen S, et al. 2020. ATP13A2-mediated endo-lysosomal polyamine export counters mitochondrial oxidative stress. *Proceedings of the National Academy of Sciences of the United States of America*, **117**(49): 31198−31207.

Vrijsen S, Houdou M, Cascalho A, et al. 2023. Polyamines in Parkinson's disease: balancing between neurotoxicity and neuroprotection. *Annual Review of Biochemistry*, **92**: 435−464.

Wang HJ, Feng TT, Guo DG, et al. 2018. Sanggenon C stimulates osteoblastic proliferation and differentiation, inhibits osteoclastic resorption, and ameliorates prednisone-induced osteoporosis in zebrafish model. *Molecules*, **23**(9): 2343.

Wang YJ, Jiang ZJ, Deng LH, et al. 2023. *Dendrobium offificinale* polysaccharides prevents glucocorticoids-induced osteoporosis by destabilizing KEAP1-NRF2 interaction. *International Journal of Biological Macromolecules*, **253**(Pt 1): 126600.

Wat WZM. 2016. Current controversies on the pathogenesis of medication-related osteonecrosis of the jaw. *Dentistry Journal*, **4**(4): 38.

Xiao J, Li WY, Zheng X, et al. 2020. Targeting 7-dehydrocholesterol reductase integrates cholesterol metabolism and IRF3 activation to eliminate infection. *Immunity*, **52**(1): 109−122.e6.

Xie BC, Zhou H, Liu HY, et al. 2023. Salidroside alleviates dexamethasone-induced inhibition of bone formation via transforming growth factor-beta/Smad2/3 signaling pathway. *Phytotherapy Research*, **37**(5): 1938−1950.

Xu XM, Liu GM, Jia G, et al. 2023. Effects of spermine on the proliferation and migration of porcine intestinal epithelial cells. *Animal Biotechnology*, **34**(2): 253−260.

Yamamoto T, Hinoi E, Fujita H, et al. 2012. The natural polyamines spermidine and spermine prevent bone loss through preferential disruption of osteoclastic activation in ovariectomized mice. *British Journal of Pharmacology*, **166**(3): 1084−1096.

Yamasaki S. 2023. Bisphosphonate use for glucocorticoid-induced osteoporosis in older patients with immune thrombocytopenia: a clinical perspective. *Annals of Hematology*, **102**(7): 1645−1656.

Yan JC, Chen S, Zhang YZ, et al. 2008. Rac1 mediates the osteoclast gains-in-function induced by haploinsufficiency of *Nf1*. *Human Molecular Genetics*, **17**(7): 936–948.

Yin H, Wang JW, Wu M, et al. 2019. Preventive effects of evodiamine on dexamethasone-induced osteoporosis in zebrafish. *Biomed Research International*, **2019**: 5859641.

Yuan CJ, Liang YC, Zhu K, et al. 2023. Clinical efficacy of denosumab, teriparatide, and oral bisphosphonates in the prevention of glucocorticoid-induced osteoporosis: a systematic review and meta-analysis. *Journal of Orthopaedic Surgery and Research*, **18**(1): 447.

Zaiss MM, Jones RM, Schett G, et al. 2019. The gut-bone axis: how bacterial metabolites bridge the distance. *Journal of Clinical Investigation*, **129**(8): 3018−3028.

Zhang LY, Li XM, Wan CF, et al. 2022. Bioinformatics analysis identification of AKT3 and RAC1 as key genes in postmenopausal osteoporosis. *Experimental and Therapeutic Medicine*, **24**(5): 656.

Zhong YT, Liao HB, Ye ZQ, et al. 2023. Eurycomanone stimulates bone mineralization in zebrafish larvae and promotes osteogenic differentiation of mesenchymal stem cells by upregulating AKT/GSK-3β/β-catenin signaling. *Journal of Orthopaedic Translation*, **40**: 132−146.

Zhou L, Song HY, Zhang YQ, et al. 2020. Polyphyllin VII attenuated RANKL-induced osteoclast differentiation via inhibiting of TRAF6/c-Src/PI3K pathway and ROS production. *BMC Musculoskeletal Disorders*, **21**(1): 112.